# AGE READING OF COD OTOLITHS BASED ON IMAGE MORPHING, FILTERING AND FOURIER ANALYSIS

Arno Formella and José M. Vázquez and Eva Cernadas
Departamento de Informática
Universidade de Vigo
Ourense, Spain
email: formella@ei.uvigo.es

Antonio Rodríguez and Germán Pérez–Gándaras
Instituto de Investigacións Mariñas
Consejo Superior de Investigaciones Científicas (CSIC)
Vigo, Spain
email: gandaras@iim.csic.es

**ABSTRACT**

We present a semi–automatic system that detects and counts the yearly growths rings of cod otoliths. The system is based on morphing an angular section of the otolith to a rectangular region where the vertical directions follow B–splines that we place with an optimization algorithm such that they cross the rings in a close to perpendicular manner. The rectangular area is treated with standard Fourier techniques and classical filters. We obtain a large number of intensity profiles which we further analyze to count the annual rings. The preliminary results achieved on a small subset of our large database are encouraging. The manual steps of the system are easy to be performed automatically as well, however, we postponed their implementation concentrating at the beginning on the global system design.

**KEY WORDS**
otolith reading, image morphing, fourier analysis.

## 1 Introduction

Age estimation of a fish population and observation of its evolution over the years becomes a more and more important task for todays fishery. One methods applied by almost all laboratories is based on the analysis of the otolith, a small bone like structure located in the ear canals of the heads of bony fish. The otolith grows during the lifetime of the fish producing ring like structures. Usually, the rings can be grouped to form yearly growth rings, or annuli, much like trees do: concentric rings around year 1 at the center. Although even daily growth can be seen. The age of the fish at the time of collection can be determined by counting the annuli. In [1] a review of the state–of–the–art in otolith reading is presented. It seems to be possible to use data on otoliths to document changes in the climate [2].

Reading of otoliths is usually done by experts in the oceanographic laboratories. There are several standard techniques available, including staining and burning of the otolith. Most of the image processing performed in the laboratories merely tries to improve the image quality and acquisition for the human expert. There exist some approaches that use image processing techniques to perform the reading in a more objective way and to deal with a larger number of otoliths.

In [3] deformable templates are used to follow the two dimensional growth of the rings. The work in [4] introduces Fourier analysis in a small area around a radial selected by the expert. Fingerprint recognition methods are used in [5] to extract 2D features that provide descriptors of the growth structures of otoliths. A Bayesian approach is taken in [6], they report a correct reading rate of 88%. Fully automated tools which are able to correctly estimate the number of annuli still have not been reported.

We present an approach, where many steps are already implemented as fully automatic, that is able to estimate the number of yearly growth rings for cod quite accurately. Preliminary results will be presented in Section 3. Our idea is as follows: we select an angular section of the otolith, this section is transformed into a rectangular area, where standard image processing techniques are used to extract the data of interest. In several phases of the algorithm filtering is employed to deal with noise, checks (false rings) and high frequency components of the ring structures.

The next section explains in detail the different steps of the image processing that starts with the original image and eventually reports the number of ages estimated for the otolith. Afterwards, we report on our preliminary results we have obtained for a randomly selected subset of the entire database.

## 2 Image processing

Our laboratory has more than 3000 otoliths which have been read manually and where some additional data, such as length of the fish, date of capture etc., has been incorporated into the database. For 690 otoliths there exist more specific data added to the database e.g., size of the otolith, thickness of its rings, type of border etc.

Our method is aimed to work with slices (usually 0.2 mm thick) which are cut from otoliths previously embedded in totally opaque polyester resin. The otolith should be cut through its longitudinal axis passing through the focus. We do not use any staining.

The images are acquired in a resolution of 2088x1550 pixels and 256 gray levels. To achieve best resolution, otoliths occupy more or less the same area within the image

independently of their actual sizes. We use a digital camera directly connected to a microscope with translucent light from below. Figure 1 shows an example of such an image.

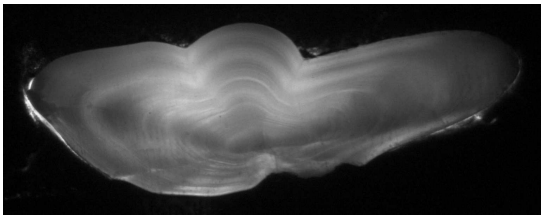

Figure 1. Original, untreated image of an otolith (1495)

The following sections describe in detail the principal steps we implemented for our age reading method. We start with an untreated gray–level image and eventually compute along a certain number of radials low pass filtered intensity values which all together are used to estimate the number of rings. Part of the processing is still performed manually. However, we do not consider this issue as a limiting factor of the method. Rather, we have postponed the development of a completely automatic system once each individual step and the final results have reached a sufficiently high level of success. Almost all manual steps could be done automatically by standard image processing tools, probably adapted to our special needs.

### 2.1 Image segmentation

The segmentation of the image consists in detecting the three areas: outer region, ring region, and core region. The outer region is the almost black area around the otolith where the light cannot pass through the preparation. The ring region (annuli) is the area which should be analyzed. The core region (nucleus) is a small area usually not located exactly in the center of the otolith where we will place later the center point. This core region is a more or less uniform gray area that does not exhibit any ring structure. We consider the detection of the nucleus the most difficult part of the segmentation process, see for instance [7] for an algorithm that intents to localize the nucleus automatically. We perform the segmentation process manually. We believe that it is easy to develop a tool that finds the outer border due to the large contrast present there. Figure 2 shows the three areas for the otolith number 1495.

### 2.2 Ring estimation

The second step computes a rough estimation of the ring structure. Discarding the outer region, we expand the histogram of the two remaining regions to enhance the contrast. (In general, all of the following operations consider only the ring and core regions of the images.) Counting from both ends of the histogram, we replace up to a small fraction of the original pixel values by the mean value of

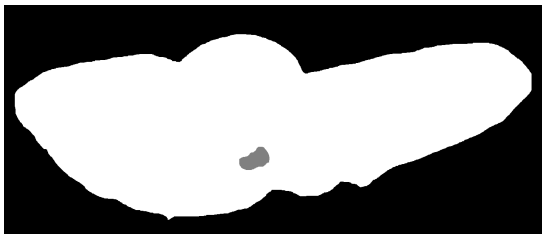

Figure 2. Image segmentation into three regions: outer region, ring region, and core region

their surrounding neighbors. Once the fraction of pixels is modified, all pixel values that have been changed but still do not fall into the center region of the histogram are replaced by the newly derived upper, respectively, lower limit of the histogram. Afterwards, we filter the region with a 3x3 mean filter maintaining the floating point values of the filter response. These values are re–quantified to 256 levels to form the enhanced image. This image is smoothed with a somewhat large mean filter (11x11). Then, we apply a conventional gradient detection with a pair of Prewitt filters which computes the angle and magnitude of the image gradient at each pixel. The angles again are smoothed through a 9x9 mean filter. Subsequently, we generate a binary image (see Figure 3) reflecting the positive and negative angle values.

Figure 3. Rough estimation of the ring structure

### 2.3 B–spline placement

Once the ring structure is roughly estimated, we manually select a central point within the previously mentioned core region. Similar to a human expert, who usually reads the age in a specific region of the otolith, we select an angular region for the subsequent steps. We believe that this step is not difficult to automate taking into account the common shape of the outer border of a cod otolith and the knowledge of the experts where the best regions are to be expected.

The outer border of the angular section is sampled with a small number (4 to 6) of equally distributed points. We place B–splines starting at the fixed center point towards the sample points on the outer border. Each B–spline interpolates its border point and the center point. Two more controls points are added to define a cubic B–spline func-

tion. Initially, we place these points equidistant along the line that connects the center point to the border point. We start an optimization procedure based on the algorithm in [8] where a derivative free minimization algorithm is described. This iterative algorithm is guaranteed to report a local minimum of the objective function within a certain tolerance in a finite number of steps. Our objective is to minimize the average of the absolute values of the dot products of the tangent vectors at the crossings of the B–splines with the estimated ring structures. In other words, we try to achieve B–splines that intersect the rings close to perpendicular. The free variables of the optimization are the locations of the inner control points and the position of the last control point on the outer border of the otolith (hence five degrees of freedom). As tangent vector at the ring structure we choose the direction that we obtain by testing all possible directions that can be computed with pixels in a square of width 41 centered at the intersection point and retaining the one where the segment with maximal minimum branch can be placed completely inside the ring. In Figure 4 the optimized B–splines for a previously selected angular section are drawn. Note that the angular section might have changed, because the end points of the left and right most B–splines might have moved.

If the minimization routine does not report a local minimum with error less than 0.1 (hence the average angle at the crossing is larger than roughly 85 degree), we start a second run. The first control point (as placed initially) is rotated around the border point until it lies on the line being normal to the border, and the second control point is chosen in the middle of the segment defined by the center point and the first control point. If, once again, the minimization routine does not report a sufficiently small local minimum, we rotate both control points such that they lie on the line being normal to the border. As last resort, we use as final B–spline the one that minimizes the error among the three trials.

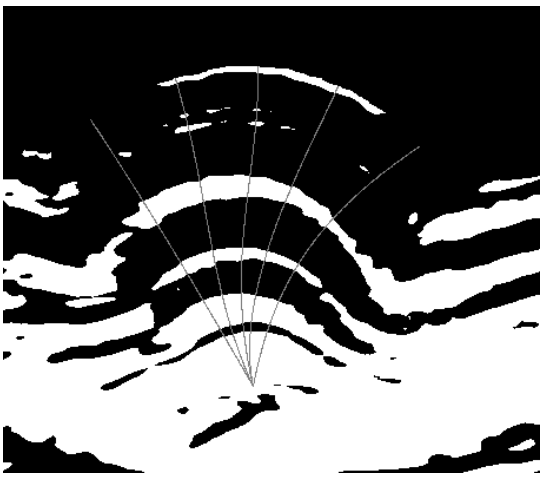

Figure 4. Guiding B–splines on the angular section where reading will take place

### 2.4 Image morphing

Once the guiding B–splines are computed, we start an image morphing step with the objective to transform the irregular shaped angular region to a rectangle. Therefore, we sample uniformly the outer border (starting at the first spline and ending at the last B–spline) and each B–spline, hence, we achieve a rectangular coordinate system spanning the region which is used for the morphing. In the current experiments, we work with a resolution of 400x500 points. For a point in this system that does not lie on a B–spline, we interpolate linearly the inner control points of the two limiting B–splines on the plane and the border control points of the splines on the border, respectively. With the help of these morphing coordinates we project the original image points onto the rectangle, where we additionally round to the closest pixel and apply a small 3x3 mean filter for noise reduction. Figure 5 shows the result of the morphing for the section of the otolith 1495 (see Figure 1 for the original image and Figure 4 for the section).

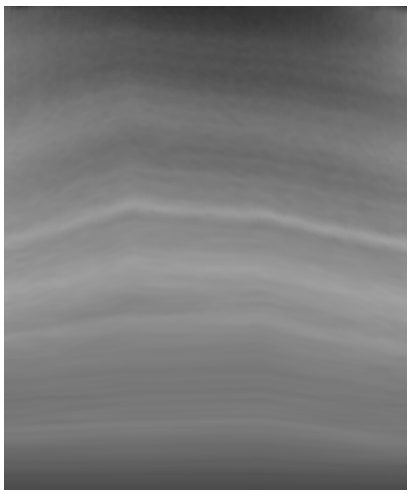

Figure 5. Image obtained after morphing of an angular section of the original image

### 2.5 Fourier analysis

Before computing a standard Fourier transformation on each column of the rectangular image, we perform a histogram expansion in the same way as already described in Section 2.2. Figure 6 demonstrates the effect of this algorithm.

We handle the complex Fourier coefficients in the following way: first, we ignore the coefficient corresponding to the zero frequency; second, we smooth the coefficients for each frequency through a row–wise mean filter of width 21; and finally we consider only the 12 coefficients standing for the lowest frequencies (low pass filtering). With these remaining complex coefficients, we reconstruct the image that we will analyze in the on–going. Figures 7 to 9

Figure 6. Image obtained after histogram expansion

visualize the three steps.

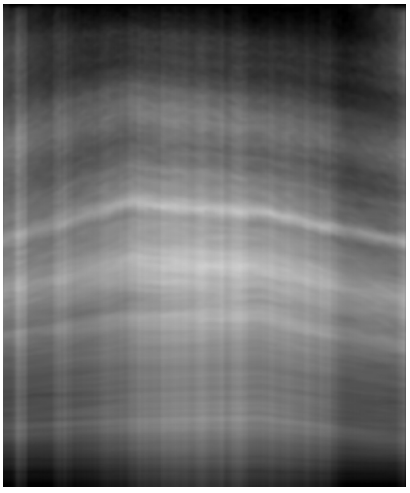

Figure 7. Reconstructed image ignoring first coefficient

Figure 8. Reconstructed image after column–wise mean filtering of complex coefficients (filter width 21 columns)

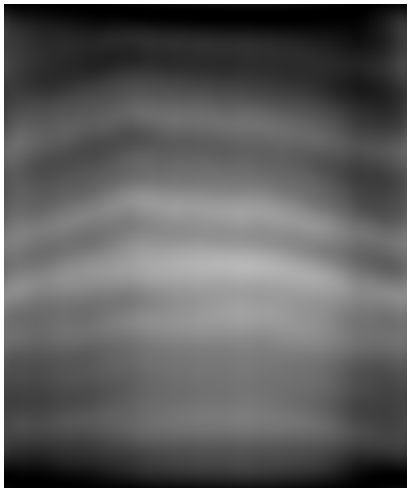

Figure 9. Reconstructed image after applying the low pass filter (for otolith 1495)

### 2.6 Age reading

In the images, once the low pass filter has been applied, one can appreciate the different bands that correspond to the annual growth of the otolith. However, simply counting the number of bands is not an adequate method for several reasons: there exists the possibility that double rings appear in certain years; there can be checks (false and incomplete rings) being present just in the selected angular region of the otolith; there can be a larger number of rings, especially close to the core region, which are produced in the first two years of life of the fish.

Here, we need more knowledge of the expert for a certain type of fish to analyze the data: for cod, usually the second year ring is the one with most prominent intensity; the thickness of the rings decreases from the core region to the outer regions; the outmost ring may be only partial depending on the season of capture; more important for the reading are prominent changes from light to dark (considering the direction from core to border) than the other way round. Note that this knowledge might be different for other type of fish.

We estimate the number of rings by an analysis of profiles which represent the columns of the image obtained after applying the low pass filter. Figure 10 shows one of these profiles (a column of Figure 9). The red disks mark the maximums points, the yellow triangles mark the minimum points, the blue squares mark decreasing slopes, and the green crosses mark the increasing slopes, (note that the x–direction in the plot is from the border to the nucleus). We placed the marks in the slopes at the location

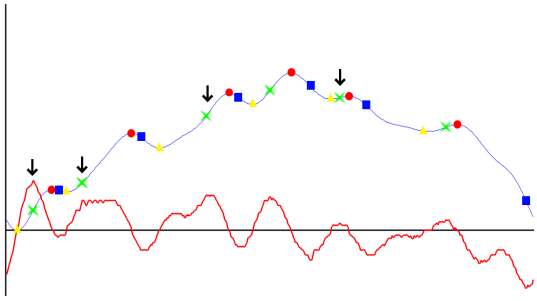

Figure 10. One column of the final region used to read the age (upper curve) and its derivative (lower curve). Here, we show a case where the system already reads correctly, otolith 1495: there appears to be a double ring for the second year.

Figure 11. Reconstructed image after applying the low pass filter (for otolith 1714)

with steepest gradients.

The number of changes from dark to light (green crosses) are counted from the outer border to the nucleus using the pre–knowledge that the width of the rings increases from the border to the nucleus. In Figure 10 the points actually counted as the end of a yearly growth ring are marked with an arrow.

We need a special treatment of the first maximum close to the border. It can happen that this first maximum is too close to the border, so the rising slope cannot be detected. However, this maximum should be considered as an additional year. In the two examples presented in the article this special case does not occur, in other cases, we take this into account.

## 3 Results

Table 1 summarizes the results that we have obtained on the randomly selected sample images of our database. Otoliths

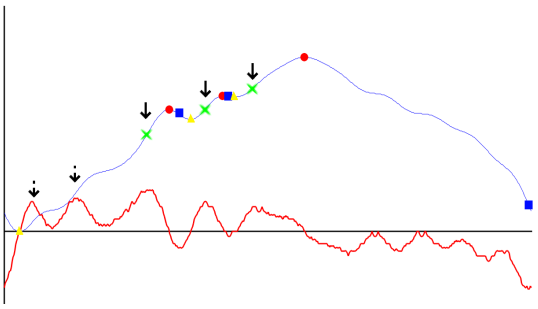

Figure 12. One column of the final region used to read the age (here, we show a case where still some improvements are required, otolith 1714)

for fish of age one and two still have been excluded. In 10 of the 17 images, the reading of the age is performed correctly. In four cases the age is subestimated by one year, and in three cases it is subestimated by two years. As described in the sequel, these subestimations are mostly due to the fact that the analysis of a column profile of the reconstructed image is still not sufficiently precise.

| number | age | estimated | $\Delta$ |
|---|---|---|---|
| 1342 | 3 | 3 | 0 |
| 1346 | (4) | 4 | 0 |
| 1409 | 3 | 3 | 0 |
| 1413 | (4) | 4 | 0 |
| 1418 | (4) | 4 | 0 |
| 1495 | 4 | 4 | 0 |
| 1499 | 4 | 3 | - |
| 1500 | 4 | 3 | - |
| 1598 | 4 | 4 | 0 |
| 1599 | 4 | 4 | 0 |
| 1602 | 4 | 4 | 0 |
| 1687 | 5 | 3 | -- |
| 1699 | 5 | 4 | - |
| 1714 | 5 | 3 | -- |
| 1792 | 5 | 4 | - |
| 1800 | 5 | 3 | -- |
| 1814 | 5 | 5 | 0 |

Table 1. Results of age reading on sample images. The table shows the number of the otolith in the database, the age as read by the human expert, the age estimated by our system, and the difference between the two ages. Three ages are set in parenthesis, because these otoliths seem to be underestimated by the expert (we re–read these otoliths in our laboratory).

The detection of the rising slope has to be improved. Currently we consider only one slope within an interval where no sign change of the first derivative occurs. However, it seems to be appropriate to count all slopes where the derivative has a sufficiently prominent maximum. This

is the reason why we still underestimate the age of otolith number 1714 by two years (see Figure 12 for a profile and Figure 11 for the filtered image). There the slopes still not counted are marked by a discontinuous arrow. The same is true for otolith number 1800. For otolith number 1687 this effect would add only one year.

Another issue that we have to improve is the localization of the increasing slopes (green crosses). Taking just the point of steepest gradient seems to be not flexible enough to place the increasing intervals expected for the ring width going from the border to the nucleus.

## 4 Conclusion

We presented a system that detects and counts quite accurately the yearly growths rings of cod otoliths. Part of the system still consists in manual work, however, we believe that these clearly identified steps can be automated easily. The system is based on morphing an angular section of the otolith to a rectangular region where the vertical directions follow B–splines that we placed perpendicular to the rings. We treated the rectangular area with standard Fourier techniques and obtained intensity profiles which we further analyzed to count the annual rings.

The results achieved on a small subset of our database are encouraging. Up to now, the system cannot read otoliths of age less than three due to the fact that there are many prominent rings in this stage of the fish development, hence, they are heavily overestimated with the current approach. Taking into account the size information of the otolith, we can possibly reduce the search space in case of otoliths of age one and two.

Further improvements of the system consist in using different types of filters (e.g., median filter) for noise reduction, improving the analysis of the slopes and their locations, possibly by introducing confidence intervals in the decision process and pre–knowledge of the relative growth rate. Clearly, we have to perform a rigorous statistical analysis using the entire database.

## Acknowledgment

This investigation was supported by the Xunta de Galicia (regional government) project PGIDIT04RMA305002PR.

## References

[1] S.E. Campana. Otolith science entering the 21st century. *Marine and Freshwater Research*, 56:485–495, 2005.

[2] G. M. Pilling, Millner R. S., M. W. Easey, D. L. Maxwell, and Tidd A. N. Phenology and north sea cod gadus morhua l.: has climate change affected otolith annulus formation and growth? *Journal of Fish Biology*, 70(2):584–599, 2007.

[3] H. Troadec, A. Benzinou, V. Rodin, and J. Le Bihan. Use of deformable template for two-dimensional growth ring detection of otoliths by digital image processing: Application to plaice (pleuronectes platessa) otoliths. *Fisheries Research*, 46:155–163, 2000.

[4] B. Morales-Nin, A. Lombarte, and B. Japón. Approaches to otolith age determination: image signal treatment and age attribution. *Scientia Marina*, 62(3):247–256, 1998.

[5] M. Palmer, A. Álvarez, A. Tomás, and B. Morales-Nin. A new method for robust feature extraction of otolith growth marks using fingerprint recognition methods. *Marine and Freshwater Research*, 56(5):791–794, July 2005.

[6] R. Fablet. Semi-local extraction of ring structures in images of biological hard tissues: application to the bayesian interpretation of fish otoliths for age and growth estimation. *Canadian Journal of Fisheries and Aquatic Science*, 63(7):1414–1428, 2006.

[7] F. Cao and R. Fablet. Automatic morphological detection of otolith nucleus. *Pattern Recognition Letters*, 27(6):658–666, 2006.

[8] U.M. García-Palomares and J.F. Rodríguez. New sequential and parallel derivative–free algorithms for unconstrained optimization. *SIAM Journal on optimization*, 13:79–96, 2002.